Available online at www.sciencedirect.com
SCIENCE DIRECT®
Journal of Solid State Chemistry 178 (2005) 1888–1897
JOURNAL OF SOLID STATE CHEMISTRY
www.elsevier.com/locate/jssc

Crystallization and second harmonic generation in thermally poled niobium borophosphate glasses

Artem Malakho[a,b,*], Marc Dussauze[a], Evelyne Fargin[a], Bogdan Lazoryak[c], Vincent Rodriguez[d], Frederic Adamietz[d]

[a]*Institut de Chimie de la Matière Condensée de Bordeaux—UPR 9048 CNRS, Chateau Brivazac, Avenue du Dr. Schweitzer, 33608 Pessac Cedex, France*
[b]*Department of Material Science, Moscow State University, Moscow 119899, Russia*
[c]*Department of Chemistry, Moscow State University, Moscow 119899, Russia*
[d]*Laboratoire de Physico-Chimie Moléculaire, UMR 5803 CNRS, Université Bordeaux I, 351 cours de la Libération, 33405 Talence Cedex, France*

Received 17 February 2005; received in revised form 19 March 2005; accepted 21 March 2005
Available online 22 April 2005

Abstract

Crystallization of glasses with compositions $(1-x)(0.95\ NaPO_3 + 0.05\ Na_2B_4O_7) + xNb_2O_5$, $x = 0.4,\ 0.43,\ 0.45,\ 0.48$ was investigated by differential scanning calorimetry and X-ray powder diffraction. Crystallization of two phases was observed in the glasses with $x = 0.43-0.48$. First phase is a sodium niobate with the structure of tetragonal tungsten bronze ($T_c \sim 720-760\,^\circ C$) and second phase is $Na_4Nb_8P_4O_{32}$ ($T_c \sim 830-850\,^\circ C$). The crystallization of sodium niobate is correlated with increasing of nonlinear optical efficiency reported for thermally poled glasses with $x > 0.4$. The results of Raman spectroscopy show the formation of three-dimensional (3D) niobium oxide framework in the glasses with increase of niobium concentration. This framework is supposed to have tetragonal tungsten bronze structure and to be responsible for nonlinear optical properties of the glass. Second harmonic generation signals of as prepared and crystallized glass after thermal poling are compared. The nucleation and crystallization do not improve the NLO properties of the glasses under study.

Keywords: Optical nonlinearity; Thermal poling; Niobium glasses; Borophosphate glasses; Glass–ceramic composites; Second harmonic generation

1. Introduction

Transparent materials with high optical nonlinearity are widely exploited in the photonic components of optical networks with high-speed information transfers. Nonlinear optical (NLO) properties are the result of nonlinear polarization induced in the material by high intensity of laser beams. The induced electric dipolar polarization can be expanded in a power series of the electric field:

$$\vec{P} = \vec{P}_{\text{linear}} + \vec{P}_{\text{nonlinear}} = \varepsilon_0\chi^{(1)}\vec{E} + \varepsilon_0[\chi^{(2)}\vec{E}\times\vec{E} + \chi^{(3)}\vec{E}\times\vec{E}\times\vec{E} + \cdots],$$

where ε_0 is the vacuum permittivity, $\chi^{(1)}$ is the linear susceptibility which accounts for the linear optical index. P_{linear} is the polarization term which is proportional to the applied field and $P_{\text{nonlinear}}$ is proportional to higher-order terms of the applied electric field. $\chi^{(2)}$ and $\chi^{(3)}$ correspond respectively to the second- and third-order nonlinear susceptibilities.

Glasses are amorphous materials with inversion symmetry on a macroscopic scale. This inversion symmetry precludes the occurrence of second-order NLO processes in the dipolar approximation.

*Corresponding author. Department of Material Science, Moscow State University, Moscow 119899, Russia. Fax: +7 095 939 21 58.
E-mail address: malakho@tech.chem.msu.ru (A. Malakho).

0022-4596/$ - see front matter © 2005 Elsevier Inc. All rights reserved.
doi:10.1016/j.jssc.2005.03.035

One possible way to initiate the NLO properties in the glass materials was found to prepare transparent composites of glasses and crystals with high optical nonlinearity. The different techniques of preparations and second harmonic generation (SHG) properties of such glass composites containing $LiNbO_3$, β-BaB_2O_4, $KTiOPO_4$ and other crystals have been reported elsewhere [1–5]. The compromise between the SHG efficiency and transparency of these materials is the key point of these investigations. The size of the particles should be in the nanoscale range and the mismatch of refractive indices for crystal and glass media has to be as small as possible.

Moreover, SHG has been observed in glasses without any crystal inclusions. The SHG signal occurs in the silica glasses after thermal or optical poling treatments [6]. For optical poling, the germanium-doped silica fiber was submitted to a long exposure of the laser irradiation such that the second harmonic efficiency grew up to nearly 5%. The thermal poling of fused silica was reported for the first time by Myers et al. [7]. This technique consists in applying a direct-current (dc) electric field below the glass transition temperature and then cooling the glass before removing the dc bias. In the result of such a procedure a nonlinear layer of 1–8 μm is created at the surface of the glass, due to space charge migration. The component of the nonlinear optical tensor d_{33} ($d_{ij} = 0.5\chi^{(2)}_{ij}$ by definition) for these layers ranges from 0 to 3 pm/V for different glasses [7–9]. These values are substantially less than those of ferroelectric crystals ($LiNbO_3$–$d_{33} \approx -34.4$ pm/V [10]) and are still not large enough to fulfil application requirements.

According to Myers et al. [7,11] two different mechanisms can be accounted for the induced second-order susceptibility $\chi^{(2)}$:

$$\chi^{(2)} = 3\chi^{(3)}E_{dc} + \Sigma Np\beta/5kT \cdot E_{loc}.$$

The first term is related to the electrical field induced inside the glass after polling coupled to the third-order susceptibility $\chi^{(3)}$. The second term arises from the possible reorientation of the N polar bonds which have a permanent dipole p, and hyperpolarizability β induced by the local field E_{loc} during the poling process.

The NLO properties of glasses may be well characterized by the magnitude of the nonlinear refractive index n_2 (related to $\chi^{(3)}$). This parameter depends on the network former anion and increases within the series F < Cl < Br < I or S < Se [6]. For oxide glasses, the lowest n_2 are obtained for silica and an increase of the values results from the introduction of "d^0" ions such as Ti^{4+}, Nb^{5+} [12,13] or heavy cations having an electronic configuration with ns^2 lone pairs (Te^{4+}, Bi^{3+}, Tl^{+}) [14]. The oxide glasses containing a large proportion of titanium or niobium oxides were investigated in detail and the magnitude of n_2 is in good agreement with the prediction deduced from the bond orbital theory given by Lines [15,16].

Recently large SHG responses were found in thermally poled borophosphate glasses $(1-x)(0.95NaPO_3 + 0.05Na_2B_4O_7) + xNb_2O_5$ with large concentration of Nb_2O_5 ($x = 35-50$ mol%). Glasses with $x \leqslant 0.40$ have nonlinear coefficient d_{33}—0.08–0.8 pm/V. For composition with $x = 0.4 - 0.5$ an extensive growth of d_{33} is observed up to 3 pm/V [9,17].

In this work the study of structure and crystallization behaviour inside these glasses is reported. The preparation of nucleated glasses and glass–ceramic composites is described in order to determine the influence of nucleation and crystallization processes on the linear and nonlinear optical properties. An explanation of the large SHG induced by thermal poling in the glasses was deduced from an investigation of their local structure and from the processes of the crystallization. Therefore the presence of structural entities closely related to that usually observed in ferroelectric crystals with tetragonal tungsten bronze-type structure is postulated to be at the origin of the high second-order optical nonlinearity typical of these glasses.

2. Experimental

2.1. Samples preparation and characterization

Glasses with compositions $(1-x)(0.95NaPO_3 + 0.05Na_2B_4O_7) + xNb_2O_5$ $x = 0.4$, 0.43, 0.45, 0.48 were prepared from commercial reagent-grade powders of $NaPO_3$ (Merck, 99.9%) $Na_2B_4O_7$ (Alfa Aesar, 99.5%) and Nb_2O_5 (Cerac, 99.99%). Stoechiometric mixtures of starting materials were melted in platinum crucible at 1300 °C for 30 min in air. The melt was poured onto the brass plate and quenched by sandwiching with another brass plate to obtain 1 mm thickness glasses. Quenched glasses were annealed at 600 °C for 24 h. As-prepared samples were cut and polished on both sides for optical transparency. Glass–ceramic composites were prepared with additional heat treatments in air of polished bulk glasses.

Thermal analyses were performed on the differential scanning calorimetry (DSC) apparatus (SSC 5400 H Seiko instruments) in the 50–950 °C temperature range for a 10°/min heating rate. Platinum was used as reference sample. The glass transition temperatures (T_g) and crystallization onset temperatures (T_c) were determined from tangent intersection of the DSC curves. The measured values of T_g and T_c were reproducible with accuracy ±5 K. Density measurements were performed using the Archimedes method with diethylorthophtalate as immersion liquid.

X-ray diffraction (XRD) patterns of initial and heat-treated samples were collected on Philips Xpert powder

diffractometer (Cu$K\alpha$—radiation, $\theta-\theta$ geometry, reflection mode) at room temperature.

The Raman spectra were recorded with a Labram confocal micro-Raman instrument (typical resolution of $3\,cm^{-1}$), in the backscattering geometry at room temperature. The spectrophotometer includes a holographic Notch for Rayleigh rejection, a microscope equipped with $100\times$ objectives, and a CCD detector. The 514.5 nm emission line of an argon ion laser was used for excitation.

2.2. Optical measurements and thermal poling

Optical transmission spectra were recorded at room temperature using double beams spectrophotometer CARY (UV-Vis-NIR) in the wavelength range 200–3000 nm. The polished samples with 500 μm thickness were used for measurements.

Thermal poling experiments were performed using the following procedure: 500 μm thick samples were sandwiched between polished silicon wafer at the anode and thin borosilicate glass plate at the cathode and then pressed on both sides by stainless steel electrodes and heated to 230 °C. The poling voltage 2 kV was applied for 30 min. Then samples were cooled down before the external voltage was removed.

Measurements of refractive indices and SHG responses were performed as described earlier [18]. The source was a Q-switched Nd/YAG laser operating at wavelength 1064 nm. The pulse width and the repetition rate of output pulses from the laser were 15 ns and 30 Hz, respectively. The polarized source beam was split into two branches by a beam splitter. One branch recorded the fundamental intensity with a Ge photodiode, the other which passed through a polarizer to adjust its polarization, was focused on the sample with a spot of 100 μm diameter. The 2ω transmitted signal was detected by a first photomultiplier and averaged over 50 pulses. The pulse energies at the sample were no more than 200 μJ for the infrared beam. The calibration of the SHG intensities is obtained using a quartz z-cut taking $d_{11}=0.3\,pm/V$ at 1064 nm as reference [19]. This versatile experimental setup allows linear refractive index to be estimated at ω or 2ω with a second photomultiplier by collecting the corresponding 2Θ reflected wave around the Brewster angle over the 10–80° Θ range. A $LiNbO_3$ crystal in phase matching condition was used as a 532 nm source. The SHG maker fringes were analyzed using the general ellipsometrical analysis for planar multilayered media [18]. The whole Maker fringe signal (in *pp* and *sp* polarization configurations, where *pp* (respectively *sp*) means *p*-polarized (respectively *s* polarized) incident pump beam and *p*-polarized transmitted second harmonic beam) was recorded for the studied samples. The determined values of the linear refractive indices were used in further simulations to allow the estimation of the nonlinear zone thickness with good accuracy. The only nonlinear coefficients which are non-zero are d_{33} and d_{31} in accordance with the polar symmetry generated by poling treatment.

3. Results

3.1. Results of DSC and XRD studies

Transparent and XRD amorphous glasses were obtained for samples with compositions $(1-x)(0.95\,NaPO_3+0.05Na_2B_4O_7)+xNb_2O_5 x=0.4$, 0.43, 0.45, 0.48 (below in the text they are marked as NBP40–NBP48).

Fig. 1 shows the results of DSC analyses for bulk glass samples. Temperatures of endothermic and exothermic effects corresponding respectively to glass transitions (T_g), and beginning of crystallization processes (T_c), as well as densities and values of cutting wavelengths for these glasses are collected in Table 1. The DSC curve for sample NBP40 glasses exhibit only one broad peak corresponding to beginning of crystallization process at

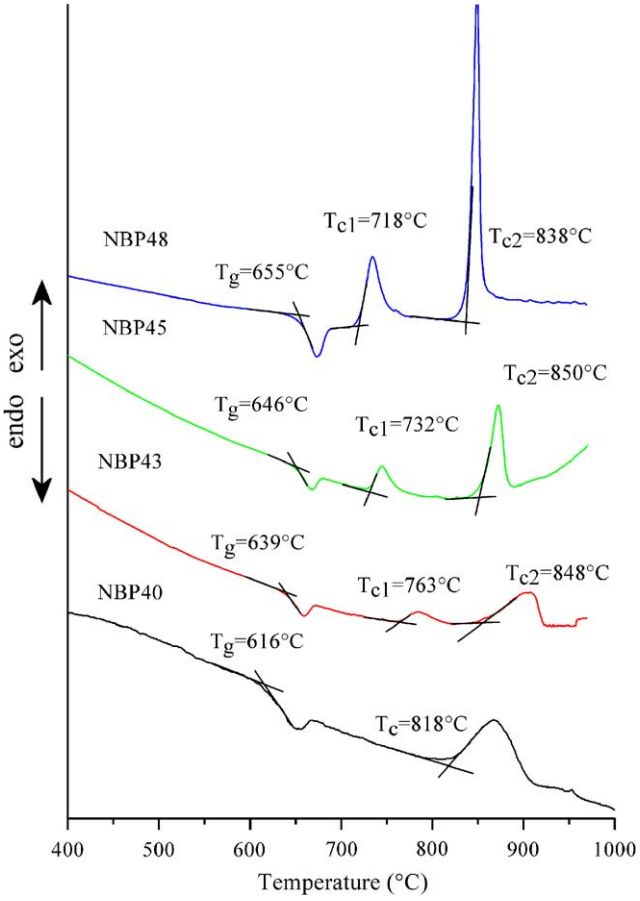

Fig. 1. DSC curves and temperatures of thermal effects for bulk samples of NBP40–48 glasses.

Table 1
Results of DSC analyses, values of density and positions of absorption edge for glasses $(1-x)(0.95\ NaPO_3+0.05Na_2B_4O_7)+xNb_2O_5$ $x=0.4$, 0.43, 0.45, 0.48

x	Sample name	T_g (°C)	T_{c1} (°C)	T_{c2} (°C)	Density (g/cm^3)	Absorption edge (nm)
0.40	NBP40	616	$T_c=818$		3.561	353
0.43	NBP43	639	763	848	3.656	355
0.45	NBP45	646	732	850	3.689	360
0.48	NBP48	655	718	838	3.750	363

~820 °C. For the samples with $x\geqslant 0.43$ two distinct crystallization effects were observed. The difference between the T_g and T_{c1} decreases for larger niobium concentration and shapes of crystallization peaks on the DSC curves become narrower. The difference between T_{c1} and T_{c2} increases from NBP43 to NBP45, and remains identical for NBP45 and NBP48.

Crystallization behavior of this glass system for compositions with $x\leqslant 0.35$ was reported earlier [20] and no crystallization was observed for glasses with $x<0.35$. For sample with $x=0.35$ (NBP35) the crystallization of $Na_4Nb_8P_4O_{32}$ was detected at temperatures above 750 °C.

The heat treatments simulating the conditions of non-isothermal crystallization during of the DSC measurements were performed for determination of crystallized phases. The XRD study of NBP40 glass heated to 900 °C (end of exothermal peak) with temperature rate 10°/min shows presence of $Na_4Nb_8P_4O_{32}$ phase only. So the broad peak on DSC curve of NBP40 glass corresponds to the crystallization $Na_4Nb_8P_4O_{32}$ and this result is in agreement with previous studies [20]. It is worth to note that the crystallization of NBP 40 glass was observed both on the surface and in the bulk.

In order to determine the phases crystallized from the glasses with two exothermal effects two samples of the NBP45 glass composition were heated from ambient temperature to the end temperature of each exothermic peak (760 and 900 °C, respectively) with rate 10°/min and then quenched in air. Then resulted samples were examined by XRD analyses. Two types of crystallization were detected in agreement with DSC data. Fig. 2 shows the XRD diagrams of two bulk NBP45 samples heated to 760 and 900 °C, respectively. Only peaks of $Na_4Nb_8P_4O_{32}$ phase present on the XRD pattern of the sample heated to 900 °C. The peaks of another phase can be observed on the XRD pattern of the sample which was heated to 760 °C.

XRD diagram of the second phase is similar to the pattern observed for phase $Na_2Nb_8O_{21}$ reported in [21] (ICDD PDF-2 pattern [13-329]) but neither crystal structure nor lattice parameters were reported for this sodium niobate and the proposed composition is not in agreement with the data of the phase diagram Nb_2O_5–$NaNbO_3$ reported in [22]. So the composition of this

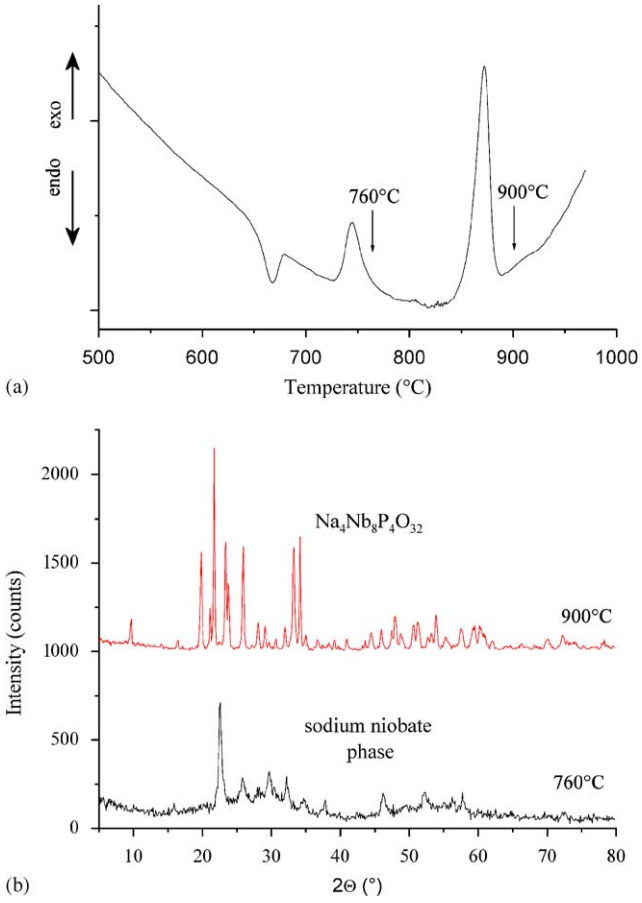

Fig. 2. The fragment of DSC curve for NBP45 glass (a) and XRD diagrams of bulk samples of NBP45 heated to 760 and 900 °C with heating rate 10°/min (b). Arrows on the DSC curve indicate the positions of heating temperatures. The XRD pattern of sample heated to 900 °C is shifted up on 1000 counts.

phase is not certainly defined. Therefore this phase will be mentioned in the text below as sodium niobate phase. Thus the first crystallization effect on the DSC curves for glasses NBP43–48 corresponds to the formation of this phase.

3.2. Crystalline phases

The phase $Na_4Nb_8P_4O_{32}$ has an elemental composition which is closed to the compositions of the richest niobium investigated glass ($x=0.48$ where Nb/

P = 1.94). This compound exhibit a monoclinic polar symmetry space group ((sp. gr.) $P2_1$, $a = 6.635$ Å, $b = 5.352$ Å, $c = 17.967$ Å, $\beta = 90.33°$, $V = 638$ Å^3, $Z = 1$) [23]. The structure is isotypic with that of monophosphate tungsten bronze $W_8P_4O_{32}$ [24]. For SHG measurements, a single-phase powder of $Na_4Nb_8P_4O_{32}$ was prepared by solid-state technique from $NaPO_3$ and Nb_2O_5 at 860 °C. The SHG patterns measured in the reflection and transmission modes were found to be rather low—in the same order of magnitude than quartz powder.

The XRD pattern of sodium niobate phase was indexed using the TREOR program. A lattice cell has been proposed in the tetragonal system with $a = 12.75(3)$ Å, $c = 5.43(1)$ Å. This calculation involves all reflexes in the 5–60° range, with a figure of merit $F_{30} = 18$ (0.0211, 48). These parameters are close to the lattice parameters of sodium tetragonal tungsten bronze (TTB) with composition $Na_{0.33}WO_3$ [25]. The TTB structure type is often observed in niobium oxides (for example $NaBa_2Nb_5O_{15}$ [26,27] or $Ba_4RNb_{10}O_{30}$, R = rare earth elements [28]).

According to the phase diagram of the Nb_2O_5–$NaNbO_3$ system reported in [22], the TTB-like non-stoechiometric phase with composition close to $NaNb_3O_8$ (Nb/Na = 3) is formed between 700 and 1280 °C. Its range of composition is temperature dependent. A line phase is reported for the composition $Na_{13}Nb_{35}O_{94}$ (Nb/Na = 2.69) [29,30]. This phase, with a related TTB structure, is ferroelectric ($T_c = 327$ K) and exhibits a superstructure (sp. gr. $Pba2$, $a = 12.364$ Å, $b = 36.992$ Å, $c = 3.955$ Å, $V = 1808.9$ Å^3, $Z = 1$). According to Abrahams [30] this phase has spontaneous polarization comparable with that of $BaTiO_3$. A complicated distribution of cations and a questionable coordination for some atomic positions of niobium are proposed for this structure. The XRD patterns of this phase and of sodium niobate phase crystallized from the glass are depicted in Fig. 3. The positions and intensities of the sub-structure lines for sodium niobate phase are found close to those of $Na_{13}Nb_{35}O_{94}$, but superstructure lines are not observed on the XRD pattern.

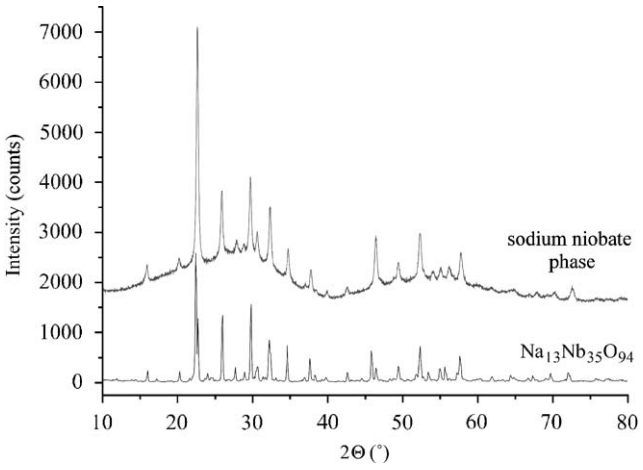

Fig. 3. XRD patterns of sodium niobate phase (crystallized glass) and $Na_{13}Nb_{35}O_{94}$. The pattern of sodium niobate phase is shifted up on 1500 counts.

According to Zhang [31] the nonlinear properties of solid solutions around the composition $NaNb_3O_8$ depends strongly on the stochiometry. Compositions rich in sodium give no SHG signal whereas an increase of the niobium concentration increases the SHG activity, which is comparable with that of KDP (KH_2PO_4).

No SHG signal was observed in crystallized glass containing sodium niobate phase as well as in $Na_{13}Nb_{35}O_{94}$ and $NaNb_3O_8$ phases prepared by solid-state technique.

3.3. Composites

The heat treatment of NBP48 samples was performed to study the influence of nucleation and crystallization processes on the optical properties of the glass. Isothermal crystallization was used as a common technique for preparation of transparent glass ceramic [32]. In the case of this type of crystallization the sample should not be quenched after heating and the transparency of them may be controlled easily.

Nucleation of glasses generates a formation of crystallization centers, i.e. nuclei. For non-metallic glasses the nucleation process usually appears at temperatures near the glass transition temperature, because it is connected with considerable molecular reconstructions in the glass. Overview of nucleation process for more than 50 silicate glass systems was performed by Fokin et al. [33] and the authors show that the maximal internal nucleation rates take place mainly at temperatures in the range 0.99–1.06 of T_g. So the nucleation may be performed by heating of glass at the temperatures closed to the glass transition temperature. The decreasing of crystallization temperature T_c is a usual result of this process. The shift of T_c may be used for quantitative study of nucleation behavior in the glass [34]. Another way to control the nucleation rate is comparison by XRD and the optical microscopy of the quantity and the size distribution of crystallites in the crystallized samples with different conditions of preliminary nucleation heating [34,35].

Nucleation of NBP48 glass ($T_g = 655$ °C and $T_{c1} = 718$ °C) was performed by heating at 680 °C for 100 h. The samples remained transparent and no crystallization was detected by XRD examination. The thermal analysis was performed to compare the crystallization temperatures of nucleated and non-nucleated samples. The decrease of $T_{c1} \sim 25$ °C was observed for nucleated sample. The following heating of this sample

at 720 °C shows the increasing of crystallization rate for nucleated glass compare to that of as-prepared glass. The appearance of crystallization was observed in the nucleated sample after 30 min of heating, whereas the as-prepared glass sample begin to crystallize only after 3 h of heating in the same conditions. These results indicate the nucleation in heated NBP48 glasses which promotes the crystallization process.

The glass ceramic composites were prepared by heating of as-prepared NBP48 samples for 5 h at 720, 730 and 740 °C. As a result, samples with different degree of transparency were obtained, from slightly opalescent (720 °C) to completely opaque (740 °C). The crystallization appears in the bulk of the glass. Only lines of sodium niobate phase could be observed on the XRD spectrum of these samples. The size of obtained crystallites is too small to be observed in the optical microscope.

3.4. UV-visible absorption spectra

UV-visible absorption spectra of as-prepared glass NBP48, nucleated glass and glass–ceramic composites are reported in Fig. 4. Within the 450–900 nm range, transparencies of as-prepared and nucleated glass are basically similar. In contrast, absorption spectra of glass ceramic composites are strongly dependent on the heating temperature (Fig. 4).

3.5. Raman spectroscopy

Fig. 5 shows the Raman spectra (500–1250 cm^{-1}) for all glass compositions. The bands corresponding to vibrations of phosphate or borate groups are weak and cannot be observed on the spectra. The strong broad band at 650 cm^{-1}, attributed to Nb–O modes with

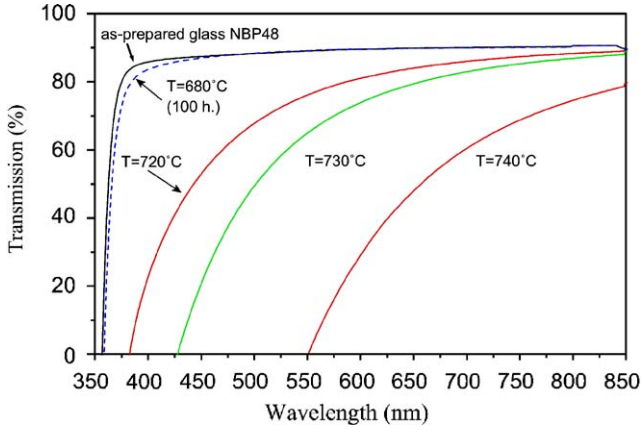

Fig. 4. Optical transmission spectra for as-prepared NBP48 glass, sample of NBP48 glass heated at 680 °C for 100 h (dashed line) and crystallized samples obtained by heating of the same glass for 5 h at the temperatures 720–740 °C.

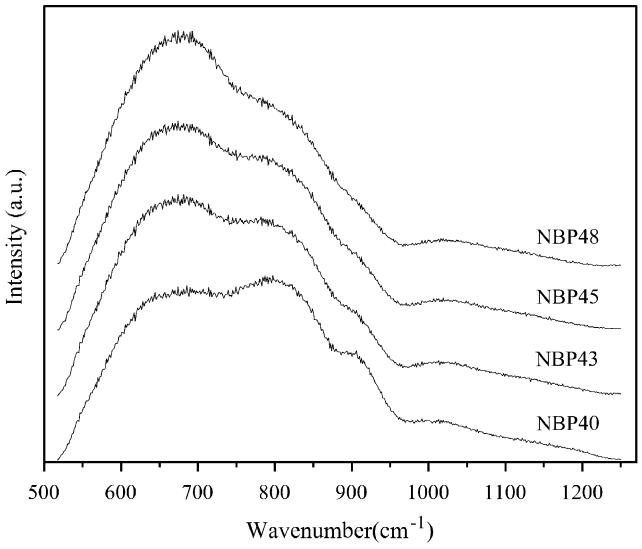

Fig. 5. Raman spectra for as-prepared NBP40-48 glasses.

Nb–O–Nb bridging, is indicative of a three-dimensional (3D) niobium oxygen framework. This band is similar to those observed in $LiNbO_3$, $NaNbO_3$ [36] and $NaBa_2Nb_5O_{15}$ [37] where NbO_6 octahedra share common corners and only Nb–O–Nb bridging is present in these structures. The intensity of this band increases with the niobium concentration. Concurrently, one may note an intensity decrease of the bands at 810 and 900 cm^{-1}. The band at 810 cm^{-1} can be attributed to modes of NbO_6 octahedra possessing both Nb–O–Nb bridging and Nb–O–P or Nb–O–B connections [17,38]. The band at 900 cm^{-1} can be attributed to Nb–O modes from distorted NbO_6 octahedra with non-bridging bonds. This band was found to be the most intensive contribution on the Raman spectra of both phosphate and silicate glasses with low concentration of niobium [38,39].

Fig. 6 reports Raman spectra for as-prepared and crystallized glasses NBP45 for different annealing times. During a heat treatment at 720 °C for 5 h, the sample becomes white opaque but we could not observe significant spectral difference between the heated and initial glass. On the other hand, the Raman spectrum of the sample heated during 22 h is characterized by a relative intensity enhancement of the band at 650 and 900 cm^{-1} as well as significant lowering of the intensity of the band at 810 cm^{-1}.

3.6. Thermal poling and SHG measurements

In order to compare the nonlinear optical properties of the three type of samples (as-prepared glass, nucleated glass and glass–ceramic composites), second harmonic generation measurements were performed before and after thermal poling. The crystallized sample with intermediate transparency ($T = 730$ °C) was taken as a representative glass–ceramic composite. No SHG

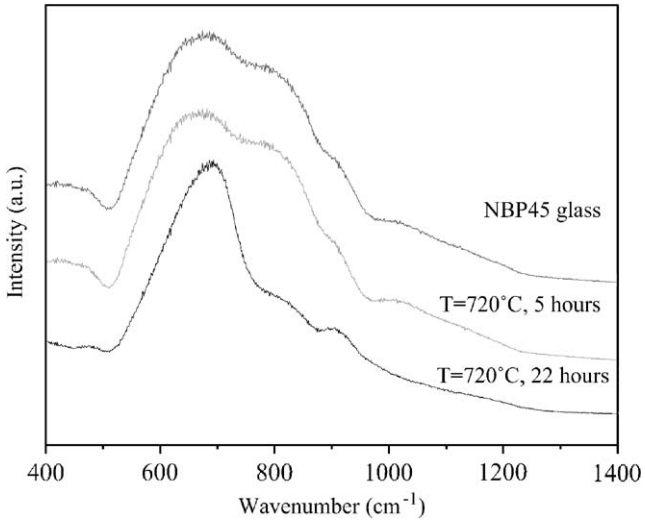

Fig. 6. Raman spectra for as-prepared NBP45 glass and the same glass crystallized by heating at $T = 720\,^{\circ}C$ for 5 and 22 h.

signal was detected for all three samples before poling. After poling, SHG signals were detected for all samples.

Maker fringe transmission spectra with *pp* and *sp* polarization were collected for as-prepared and nucleated glass samples. Basically, SHG patterns are similar to those of a bulk poled glass; they correspond to a second-order optical nonlinearity localized in a thin layer at the anode surface of poled glass. Experimental and calculated patterns with both *pp* and *sp* polarization scheme are presented in Fig. 7. The optical parameters obtained from a complete analyze of the Maker fringes of these two samples are summarized in the Table 2. All the obtained parameters for as-prepared glass are in good agreement with the values reported earlier [17]. Despite of an increase of the linear refractive index, the d_{33} susceptibility of the nucleated sample is smaller than that obtained for the as-prepared glass.

The SHG study of the glass–ceramic composite was performed in order to evaluate the influence of the crystallization on the optical nonlinear activity and also to check the SHG efficiency of the crystallized phase after thermal poling. Fig. 8 shows the *pp* polarized transmission and reflection spectra of poled glass ceramic composite; the same SHG polarized pattern of poled NBP48 glass is reported for comparison. The SHG signal of poled composite completely disappears after removing (by polishing) of the ~20 μm layer on the anodic surface of the sample.

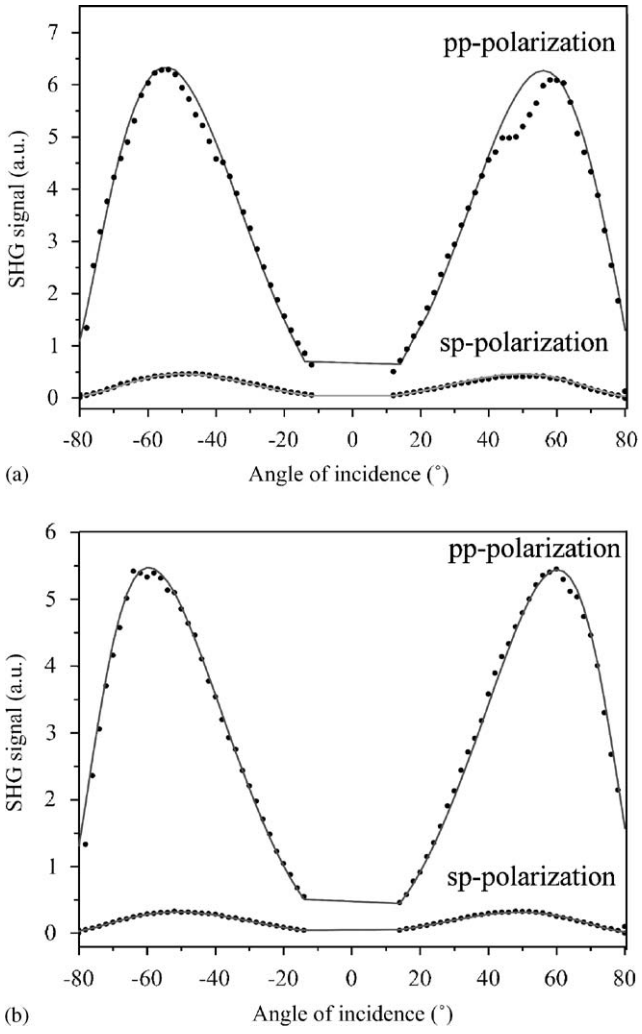

Fig. 7. Experimental (points) and calculated (solid lines) transmitted SHG Maker-fringe patterns for as-prepared NBP48 (a) and nucleated sample NBP48 (b), both poled 30 min at 230 °C with 2 kV.

4. Discussion

4.1. Structure of the materials

From the analysis of Raman spectra and the crystallization process, the evolution of the glass structure can be explained by a modification of the niobium oxygen framework.

The glass-former is made up of the Nb–O, P–O, and B–O structural entities and the sodium ions are assumed to be modifiers. The niobium is located in NbO_6 octahedra that can be connected either with other NbO_6 units, P–O or B–O entities, or with sodium. The structural peculiarities of glasses $(1-x)(0.95NaPO_3 + 0.05Na_2B_4O_7) + xNb_2O_5$ $(x = 0-43)$ were studied extensively by Raman, EXAFS and IR spectroscopes [17,38]. EXAFS study shows the octahedral coordination of Nb for all studied compositions [38]. The increasing of niobium concentration leads to decompositions of polyphosphate chains on the isolated PO_4^{3-} and $P_2O_7^{4-}$ groups [17]. The formation of 3D units of NbO_6 octahedra was found from the Raman and IR investigations [17,38]. The aim of this work was to study this arrangement of NbO_6 octahedra for glasses with rich niobium concentration and to found the

Table 2
Values of nonlinear coefficients d_{33} and d_{31}, thickness of nonlinear layer and refractive indices for thermally poled samples of as prepared and nucleated NBP48 glass

Sample	d_{33} (pm/V)	d_{31} (pm/V)	Nonlinear layer (μm) (±10%)	Refractive index n	
				$\lambda = 1064$ nm	$\lambda = 532$ nm
As-prepared NBP48	2.1 (1)	0.7	3.0	1.92 (1)	2.00 (1)
Nucleated NBP48	1.9 (1)	0.63	2.8	1.95 (1)	2.02 (1)

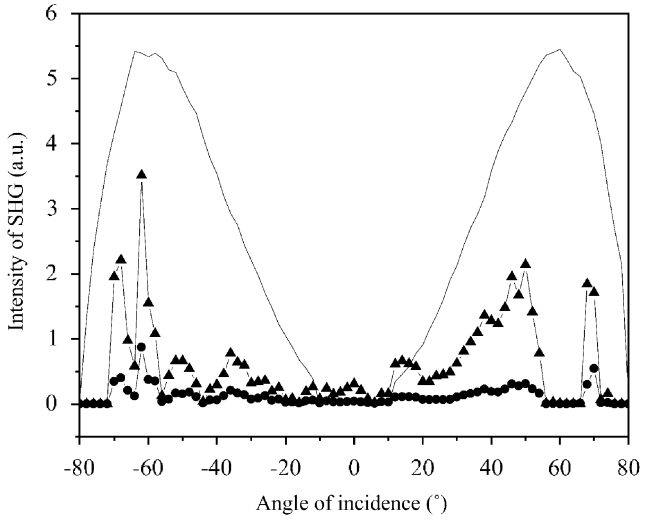

Fig. 8. Reflection (triangles) and transmission (circles) SHG patterns of poled sample of NBP48 glass crystallized at 730 °C for 5 h. Transmission SHG pattern of as-prepared poled NBP48 glass is given for comparison (solid line).

correlations with results of crystallization and optical nonlinearity of these glasses.

Three main bands are observed on the Raman spectra at 650, 810 and 900 cm^{-1}. The first one corresponds to the niobium oxygen octahedral surrounded by the six other niobium oxygen octahedra. The second one corresponds to Nb–O bond in NbO_6 octahedra with Nb–O–P bridging and the third band corresponds to the NbO_6 octahedra with several non-bridging bonds. The intensity ratios of the 650 cm^{-1} band over both 810 and 900 cm^{-1} bands increase with the niobium concentration. The evolution of the Raman spectra with niobium loading can be explained by an extension of 3D arrangement of NbO_6 octahedra sharing common corners. The constructions of this arrangement cannot be revealed only by spectroscopy methods. Raman spectra of crystalline phases with structures made of different 3D NbO_6 units (for example $Na_4Nb_8P_4O_{32}$ [20], $NaNbO_3$ [36] and $NaBa_2Nb_5O_{15}$ [37]) exhibit the same bands at the 600–670 cm^{-1}.

However, the glass compositions are close to the composition of the $Na_4Nb_8P_4O_{32}$ phase. In such a structure, the layers of NbO_6 octahedra are alternated by isolated PO_4 groups and sodium cations (Fig. 9). The crystallization of this phase occurs at temperature higher than 800 °C for all studied compositions. The thermal analyses reveal a large difference (~200–230 °C) between T_g and T_{c2}. Therefore, high activation energy is required to crystallize the $Na_4Nb_8P_4O_{32}$ phase and this transformation involves substantial displacements of the atoms from their initial glassy local structure. The crystallization of sodium niobate phase is effective for glass samples with $x > 0.40$ at lower temperature T_{c1}, which is very close to T_g. For these glasses, a smaller amount of activation energy is required to transform partially the glass into this type of crystal state and the smaller atomic displacements occur at this transformation. The Fig. 6 shows the Raman spectra of initial NBP45 glass and glasses crystallized at 720 °C for 5 and 22 h. No changes on the Raman spectra were found after heating for 5 h despite the appearance of crystalline phase and lost of transparency of the sample. Thus the arrangement of 3D niobium units is not changes on the first steps of crystallization. The difference of Raman spectra may be observed for sample crystallized for 22 h. Intensive crystallization initiates enhancement of bands at 650 and 900 cm^{-1} and weakening of the band at 810 cm^{-1}. These changes can be explained as the separation of the crystallites of sodium niobate phase (band at 650 cm^{-1}) from the glass matrix with low niobium concentration characterized by band at 900 cm^{-1} [38].

Besides our results, an increase of the d_{33} nonlinear susceptibility from 0.8 to 3 pm/V, for glass compositions with $x > 0.40$, has been reported elsewhere [9,17]. Indeed, the highest SHG responses were obtained for poled glasses with composition where the crystallization of sodium niobate phase takes place. This correlation is similar with results of Lipovskii et al. [39,40], who associate the increasing of electro optical response in the niobium silicate glasses with formations of crystalline ordering in small regions (2–3 coordination spheres) with arrangement of the atoms similar with structures of electro optical crystals [40].

From a preliminary XRD investigation, we have found that the structure of this sodium niobate phase is related to that of tetragonal tungsten bronze. Ferroelectric properties and nonlinear optical activity is

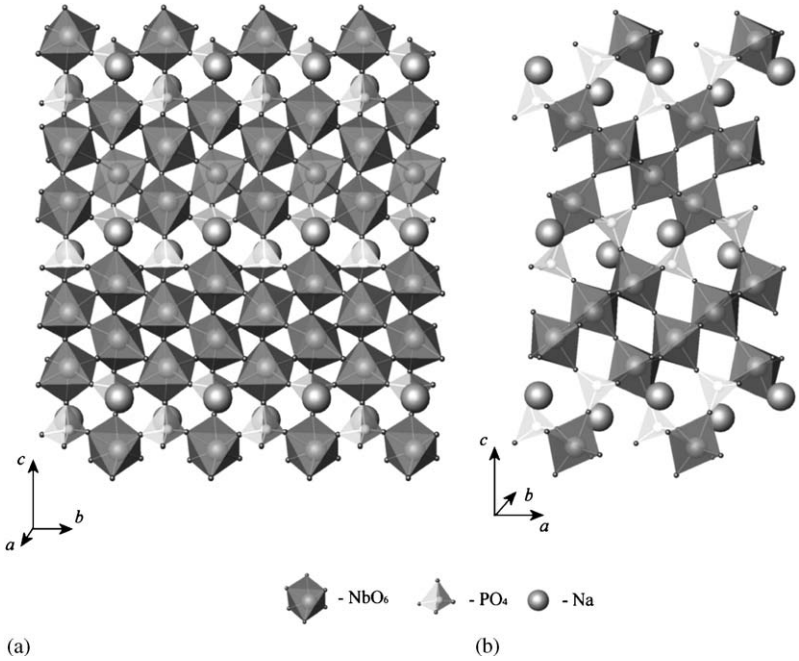

Fig. 9. Polyhedral views of the $Na_4Nb_8P_4O_{32}$ structure along the [100] (a) and [010] (b) directions [23].

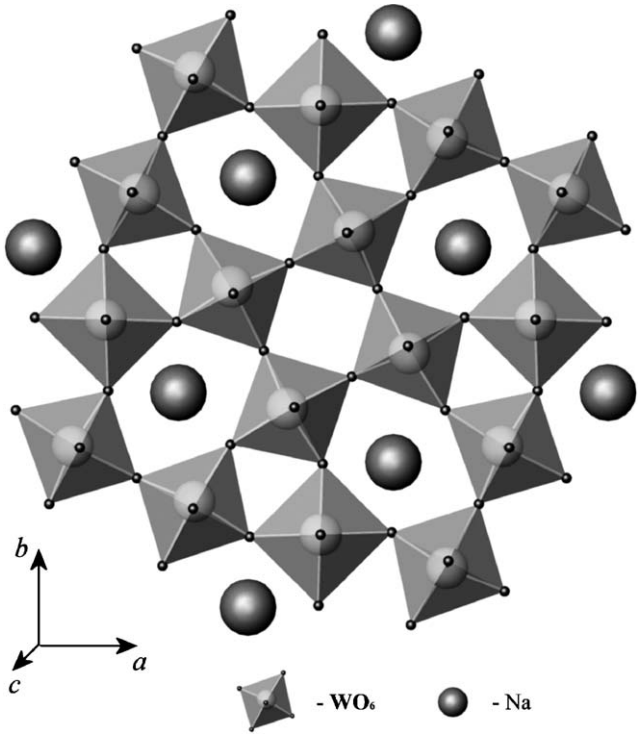

Fig. 10. A polyhedral view along the [001] direction for the crystal structure of tetragonal tungsten bronze $Na_{0.33}WO_3$ [25].

observed for niobate crystals with this structural type (for example $NaBa_2Nb_5O_{15}$ [27]). The polyhedral view of TTB structure for $Na_{0.33}WO_3$ is presented in Fig. 10. This structure exhibit a channel framework $\{M_5O_{15}\}_n$ ($M = W$, Nb) made up of MO_6 octahedra sharing common corner. The channels in this structure are occupied by the metal cations. Therefore it can be inferred that the local glass structure has similar arrangement of NbO_6 octahedra as that of TTB bronze probably with a composition close to $NaNb_3O_8$.

4.2. Nonlinear optical properties of the materials

The study of nucleated and crystallized glass samples shows the negative influence of the crystalline inclusions on the optical properties of glasses and glass–ceramic composites. The nucleation process does not change the optical properties of glass. However, the Raman and XRD studies also do not reveal significant difference between as-prepared and nucleated samples. Therefore, the nucleation does not modify efficiently the local arrangement of atoms in the glass. The optical properties as refractive indices, absorption spectra and nonlinear optical activity differ slightly for as-prepared and nucleated glasses. The results obtained from the analyses of the SHG patterns indicate that nucleation does not improve the NLO response. Only a slight decrease of SHG activity and some increasing of absorption could be observed after nucleation.

The loss of transparency is the main result of the crystallization (Fig. 4). The crystallized glasses are characterized by a strong scattering increase with the heating temperature in the SHG spectral range. Moreover, the transmitted and reflected SHG patterns are quite comparable although the transmitted signal intensity is lower due to strong scattering effects. Nevertheless, the overall shape of these patterns seems to be comparable to the SHG pattern of as-prepared poled glass. The nonlinear layer at the anodic surface of the sample is thought to be the main source of SHG

response, both in poled as-prepared and nucleated glasses because no SHG signal was detected after removing of this layer by polishing. The crystalline part of the nucleated and crystallized glasses has no obvious influence on the SHG activity.

5. Conclusions

Crystallization behavior for glasses with compositions $(1-x)(0.95NaPO_3+0.05Na_2B_4O_7)+xNb_2O_5$ $x=0.4$, 0.43, 0.45, 0.48 was investigated. Two types of phases were found to crystallize in this range of composition. For glasses with lower SHG efficiency ($x=0.35-0.40$) a crystallization of only one phase—$Na_4Nb_8P_4O_{32}$ was observed above 800 °C. For glasses with $x=0.43-0.48$, a crystallization of another phase was found between 700 and 800 °C. This phase is a sodium niobate with structure of tetragonal tungsten bronze. Nucleation of sodium niobate phase was performed in order to study the optical properties of nucleated glass. Glass–ceramic composites with different transparency were prepared. The SHG properties of initial, nucleated and partially crystallized glasses were compared before and after thermal poling. It was found that either nucleation or crystallization do not improve the SHG response of the glasses. The local glass structure is supposed to have a structural arrangement rather close to that of the TTB bronze for the richest niobium glasses with $x>0.43$. Such arrangement of the NbO_6 octahedra in the glass structure is necessary to induce high second-order optical nonlinearity after thermal poling.

Acknowledgments

We acknowledge the program ACI nanosciences–nanotechnologies (2000) for financial support. A.M. is grateful to the French government for the scholarship. V.R. is indebted to the Région Aquitaine for financial support in optical, laser, and computer equipment.

References

[1] Y. Ding, A. Osaka, Y. Miura, H. Toratani, Y. Matsuoka, J. Appl. Phys. 77 (1995) 2208.
[2] Y.E. Tsai, Y.H. Chang, K.Y. Lo, Mater. Sci. Eng. A 293 (2000) 229.
[3] Y.H. Kao, Y. Hu, H. Zheng, J.D. Mackenzie, K. Perry, G. Bourhill, J.W. Perry, J. Non-Cryst. Solids 167 (1994) 247.
[4] V.N. Sigaev, P. Pernice, A. Aronne, O.V. Akomova, S.Yu. Stefanovich, A. Scaglione, J. Non-Cryst. Solids 292 (2001) 59.
[5] D. Li, L. King, L. Zhang, X. Yao, J. Non-Cryst. Solids 271 (2000) 45.
[6] E.M. Vogel, M.J. Weber, E.M. Krol, Phys. Chem. Glasses 32 (1991) 231.
[7] R.A. Myers, N. Mukherjee, S.R.J. Brueck, Opt. Lett. 16 (1991) 1732.
[8] A. Narazaki, K. Tanaka, K. Hirao, N. Soga, J. Appl. Phys. 83 (8) (1998) 3986.
[9] M. Dussauze, E. Fargin, M. Lahaye, V. Rodriguez, F. Adamietz, Opt. Express, submitted.
[10] V.G. Dmitriev, G.G. Gurzadyan, D.N. Nikogosyan, Handbook of Nonlinear Optical Crystals, Springer, Berlin, 1991.
[11] N. Mukherjee, R.A. Myers, S.R.J. Brueck, J. Opt. Soc. Am. B 11 (1994) 665.
[12] E. Fargin, A. Berthereau, T. Cardinal, G. Le Flem, L. Ducasse, L. Canioni, P. Segonds, L. Sarger, A. Ducasse, J. Non-Cryst. Solids 203 (1996) 96.
[13] T. Cardinal, E. Fargin, G. Le Flem, M. Couzi, L. Canioni, P. Segonds, L. Sarger, A. Ducasse, F. Adamietz, Eur. J. Solid State Inorg. Chem. 33 (1996) 597.
[14] B. Jeansannetas, S. Blanchandin, P. Thomas, P. Marchet, J.C. Champarnaud-Msjard, V. Nazabal, E. Fargin, G. Le Flem, M.O. Martin, B. Bousquet, L. Canioni, S. Le Boiteux, P. Segonds, L. Sarger, J. Solid State Chem. 146 (1999) 329.
[15] M.E. Lines, Phys. Rev. B 43 (1991) 11478.
[16] L. Sarger, P. Segonds, L. Canioni, F. Adamietz, A. Ducasse, C. Duchesne, E. Fargin, R. Olazcuaga, G. Le Flem, J. Opt. Soc. Am. B 11 (1994) 995.
[17] M. Dussauze, E. Fargin, A. Malakho, V. Rodriguez, T. Buffeteau, F. Adamietz, Opt. Mater., in press.
[18] V. Rodriguez, C. Sourisseau, J. Opt. Soc. Am. B 19 (2002) 2650.
[19] M.G. Kuzyk, C.W. Dirk, Characterization Techniques and Tabulations for Organic Nonlinear Optical Materials, Marcel Dekker Inc., New York, 1998.
[20] J.J. Videau, T. Cardinal, G. Le Flem, Phosophorus Res. Bull. 10 (1999) 646.
[21] M.W. Shafer, R. Roy, J. Am. Ceram. Soc. 42 (1959) 482.
[22] R.S. Roth, H.S. Parker, W.S. Brother, D.B. Minor, Alkali oxide-tantalum oxide and alkali oxide-niobium oxide ionic conductors. NASA Contract Rep. # NASA-CR-134599, NASA, Cleveland, OH, 1974, pp. 1–59.
[23] G. Constentin, M.M. Borel, A. Grandin, A. Leclaire, B. Raveau, Mater. Res. Bull. 26 (1991) 1051.
[24] J.P. Giroult, M. Goreaud, Ph. Labbé,, B. Raveau, Acta Crystallogr. B 37 (1981) 2139.
[25] F. Takusagawa, R.A. Jacobson, J. Solid State Chem. 18 (1976) 163.
[26] A. Magneli, Ark. Kemi. 1 (1949) 269.
[27] P.B. Jameison, S.C. Abrahams, J.L. Bernstein, J. Chem. Phys. 50 (1969) 4352.
[28] O.G. D'yachenko, S.Ya. Istomin, M.M. Fedotov, E.V. Antipov, M. Nygren, W. Holm, G. Svensson, Mater. Res. Bull. 32 (4) (1997) 409.
[29] D.C. Craig, N.C. Stephenson, J. Solid State Chem. 3 (1971) 89.
[30] S.C. Abrahams, C.D. Brandle, G.W. Berkstresser, H.M. O'Bryan, H.E. Bair, P.K. Gallagher, J. Appl. Phys. 65 (4) (1989) 1797.
[31] W.Z. Zhang, W. Liu, H.Y. Shen, Appl. Phys. Lett. 58 (1991) 2334.
[32] H. Jain, Ferroelectrics 306 (2004) 111.
[33] V.M. Fokin, E.D. Zanotto, J.W.P. Schmelzer, J. Non-Cryst. Solids 321 (2002) 52.
[34] T. Wakasugi, L.L. Burgner, M.C. Weinberg, J. Non-Cryst. Solids 244 (1999) 63.
[35] J. Deubener, J. Non-Cryst. Solids 274 (2000) 195.
[36] Y.D. Juang, S.B. Dai, Y.C. Wang, W.Y. Chou, J.S. Hwang, M.L. Hu, W.S. Tse, Solid State Commun. 111 (1999) 723.
[37] S.D. Ross, J. Phys. C: Solid State Phys. 3 (1970) 1785.
[38] T. Cardinal, E. Fargin, G. Le Flem, S. Leboiteux, J. Non-Cryst. Solids 222 (1997) 228.
[39] A.A. Lipovskii, D.K. Tagantsev, A.A. Vetrov, O.V. Yanush, Opt. Mater. 21 (2003) 749.
[40] A.A. Lipovskii, D.K. Tagantsev, B.V. Tatarintsev, A.A. Vetrov, J. Non-Cryst. Solids 318 (2003) 268.